

Effect of wave paddle motions on water waves

Hui Liang, Yun Zhi Law, Harrif Santo, Eng Soon Chan

Technology Centre for Offshore and Marine, Singapore (TCOMS), 12 Prince George's Park, 118411.

E-mail: liang_hui@tcoms.sg

1 Introduction

A fully-nonlinear numerical wave tank equipped with hinged-flap wave paddles is set up by means of the 3D Harmonic Polynomial Cell (HPC) method in the time domain. Three kinds of wave-making boundary conditions, including: the smooth velocity distribution, discrete velocity inlet and discrete paddle motions, are investigated. Numerical results show that the staggered motion of wave paddles produces an additional radiation wave field and this wave system poses a non-negligible influence on higher harmonic wave components.

2 Summary of the 3D time-domain HPC method

The potential-flow based HPC method is proposed by Shao and Faltinsen [1, 2], and it is extensively studied in recent years [3–5]. The fluid domain is discretized into overlapping hexahedral cells, and each stencil cell is defined as the combination of 8 neighboring hexahedral cells with 27 grid points. The velocity potential within each cell is represented as a linear combination of harmonic polynomials:

$$\phi(x, y, z) = \sum_{j=1}^{26} b_j \mathcal{P}_j(x, y, z) \quad (1)$$

where \mathcal{P}_j ($j = 1, \dots, 26$) mean harmonic polynomials associated with Legendre polynomials in a spherical coordinate system [2]. By imposing equation 1 on the 26 stencil points, one can obtain a linear equation system in the form of:

$$[\mathbf{A}] \cdot \{\mathbf{b}\} = \{\phi\} \quad \text{with} \quad A_{i,j} = \mathcal{P}_j(x_i, y_i, z_i) \quad (2)$$

By taking the inverse of (2), we can obtain the vector $\{\mathbf{b}\}$:

$$b_i = \sum_{j=1}^{26} c_{i,j} \phi_j \quad \text{with} \quad i = 1, \dots, 26 \quad (3)$$

where $c_{i,j}$ ($i, j = 1, \dots, 26$) are elements of the inverse of the matrix $[\mathbf{A}]$. Substituting (3) into (1) gives rise to:

$$\phi(x, y, z) = \sum_{i=1}^{26} \left[\sum_{j=1}^{26} c_{i,j} \phi_j \right] \mathcal{P}_i(x, y, z) = \sum_{i=1}^{26} \left[\sum_{j=1}^{26} c_{j,i} \mathcal{P}_j(x, y, z) \right] \phi_i \quad (4)$$

Equation (4) indicates that the velocity potential at any point in the cell can be interpolated by the velocity potential on the surrounding nodes of the cell. By setting $x = x_{27} = 0$, $y = y_{27} = 0$ and $z = z_{27} = 0$, one can obtain the following equation

$$\phi_{27} = \sum_{i=1}^{26} c_{1,i} \phi_i \quad (5)$$

indicating the continuity of the flow through the cell. On the solid boundaries, the Neumann-type condition requiring the derivative of the potential is implemented by directly taking the derivative of harmonic polynomials in (4).

On the free surface, the Diriclet-type condition is satisfied via prescribing the velocity potential on the nodes. On the free surface away from wave paddles, a semi-Lagrangian description which tracks a

vertically moving point is applied with dynamic and kinematic free-surface boundary conditions given by:

$$\frac{d^s \phi}{dt} = -g\zeta - \frac{1}{2} \left(\frac{\partial \phi}{\partial x} \right)^2 - \frac{1}{2} \left(\frac{\partial \phi}{\partial y} \right)^2 + \frac{1}{2} \left(\frac{\partial \phi}{\partial z} \right)^2 - \frac{\partial \phi}{\partial x} \frac{\partial \zeta}{\partial x} \frac{\partial \phi}{\partial z} - \frac{\partial \phi}{\partial y} \frac{\partial \zeta}{\partial y} \frac{\partial \phi}{\partial z} \quad \text{on } z = \zeta(x, y, t) \quad (6a)$$

$$\frac{d^s \zeta}{dt} - \frac{\partial \phi}{\partial z} + \frac{\partial \phi}{\partial x} \frac{\partial \zeta}{\partial x} + \frac{\partial \phi}{\partial y} \frac{\partial \zeta}{\partial y} = 0 \quad \text{on } z = \zeta(x, y, t) \quad (6b)$$

where ζ means the free-surface elevation.

Near wave paddles, the Lagrangian description tracking the motion of fluid particles is adopted, and the dynamic and kinematic free-surface boundary conditions are:

$$\frac{d\mathbf{x}}{dt} = \nabla \phi \quad \text{on } z = \zeta(x, y, t) \quad (7a)$$

$$\frac{d\phi}{dt} = -g\zeta + \frac{1}{2} |\phi|^2 \quad \text{on } z = \zeta(x, y, t) \quad (7b)$$

The explicit 4th-order Runge-Kutta scheme is used to integrate the boundary conditions (6) or (7) to update the potential and elevation of the free surface at each time step. To ensure stability, a 11-point, 8th-order Savitzky-Golay filter [6] adopted in [7] is used to remove possible saw-tooth waves.

3 Results and discussions

Based on the 3D time-domain HPC method, a square numerical wave tank, 9.6m by 9.6m by 1.5m depth, is set up as shown in Fig. 1. Hinged-flap wave paddles with 0.5m width and 1m draft are uniformly distributed along the top side and absorbing beaches are introduced on the left-hand and bottom sides. Between two adjacent paddles, there is a gap with the width 0.1m.

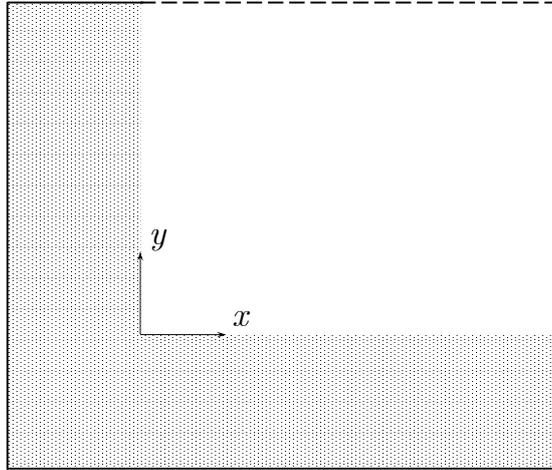


Figure 1: Sketch of a square numerical wave tank. The dashed line means wave paddles, and the shadow part represents the damping zone.

Oblique waves generated by wave paddles along the top side are now considered. To generate an oblique wave system with the propagation angle β , the instantaneous pitch angle of the paddle j is written as [8]:

$$\xi_j = a \sin(\omega t - k_0 y_j \sin \beta) \quad (8)$$

where y_j means the coordinate in y -direction of the centroid of the wave paddle j , and wave frequency ω and wavenumber k_0 are subjected to the dispersion relation in finite wave depth.

Here, three kinds of wave-making boundary conditions are considered, including: (1) a smooth velocity distribution along the wave-making boundary; (2) a discrete velocity distribution subjected to the width of the wave paddle; (3) discrete paddle motions. In the first two boundary conditions, the

paddle boundary condition is satisfied on the mean position, whereas the third one is imposed on the instantaneous position.

Fig. 2 shows the plan view of wave patterns at the time instant $t = 20$ s. The results obtained from (1) smooth velocity distribution, (2) discrete velocity distribution and (3) discrete paddle motions are placed on the left, middle and right columns, respectively. The wave frequency is $\omega = 4$ rad/s corresponding to the wavelength $\lambda = 3.85$ m, and the propagation angle is $\beta = -30^\circ$ with respect to the negative y -axis.

By observing Fig. 2, there is no obvious difference between the results obtained from wave-making boundary conditions (1) and (2). Nevertheless, the results associated with the boundary condition (3) exhibit distinguishable discrepancies. The contour lines are not smooth indicating the presence of short waves. These short waves are associated with the radiation wave field due to the motion of wave paddles.

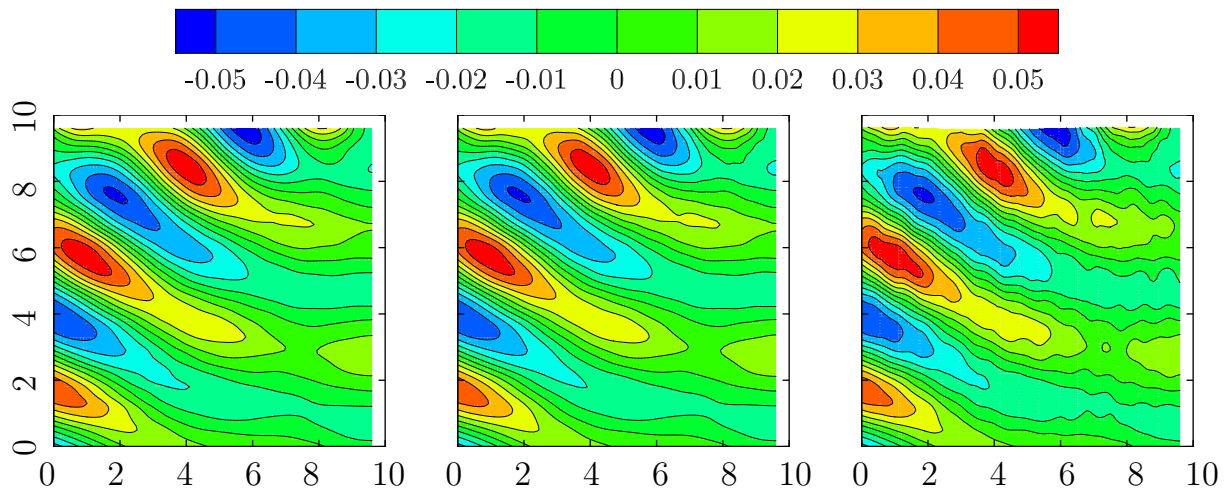


Figure 2: Plan view of generated wave patterns obtained from the smooth velocity distribution (left column), discrete velocity distribution (middle column) and discrete paddle motions (right column) at the time instant $t = 20$ s. The wave frequency is $\omega = 4$ rad/s, and the propagation angle is $\beta = -30^\circ$ with respect to the negative y -axis.

Fig. 3 illustrates the difference between wave fields associated with the discrete velocity distribution and discrete paddle motions which are shown in the middle and right parts of Fig. 2. It can be clearly observed that their difference yields only short waves, and the amplitude of short waves is about 6% of the amplitude of the reference wave field.

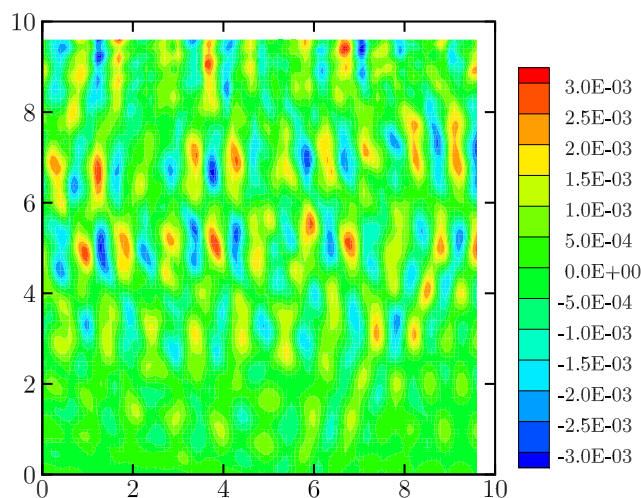


Figure 3: The difference between wave fields obtain from discrete velocity distribution and discrete paddle motions.

To delve into the effect of paddle motions on the wave field, we perform the FFT to the time series of the free-surface elevation at a probed location $(x, y) = (1.0, 6.0)$ for both discrete velocity distribution

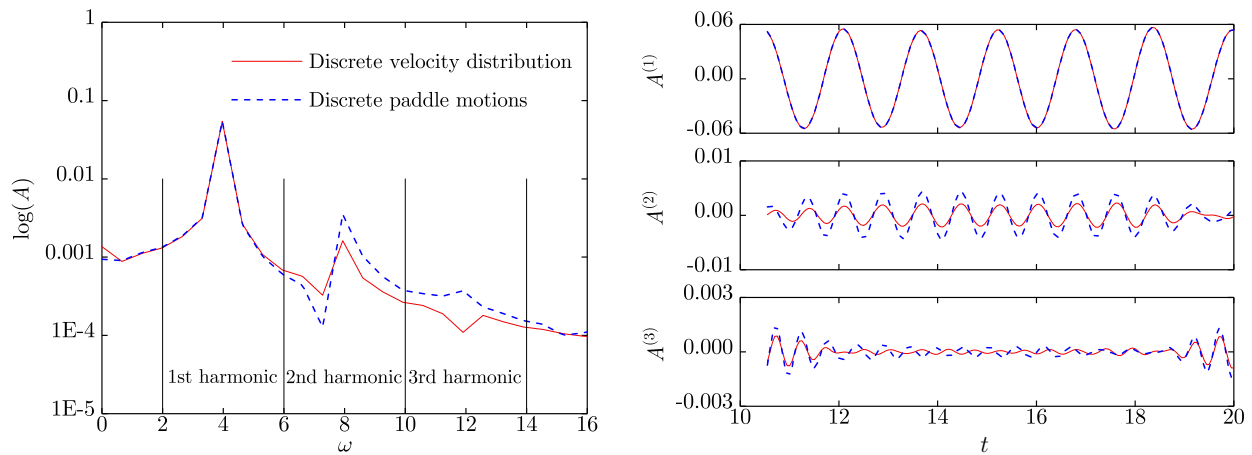


Figure 4: FFT to the time series of the free-surface elevation at $(x, y) = (1.0, 6.0)$ (left); the first, second and third harmonics determined by the inverse FFT (right).

and discrete paddle motions as shown in the left part of Fig. 4. It can be observed that the paddle motions hardly affect the first harmonic component, while they pose non-negligible influences on the second and third harmonics. In the right part of Fig. 4, the time series due to the first, second and third harmonics are plotted using the inverse FFT technique. The differences in the time series associated with the second and third harmonics confirm this finding.

This work is an ongoing work, waves generated by two-sided wave paddles will be considered to study the interactions between waves and staggered paddle motions. These results will be presented at the workshop.

4 Acknowledgment

This research is supported by A*STAR Science and Engineering Research Council, Grant number 172 19 00089 under the Marine & Offshore Strategic Research Programme (M&O SRP).

References

- [1] Y. L. Shao and O. M. Faltinsen, “Towards efficient fully-nonlinear potential-flow solvers in marine hydrodynamics,” in *Proceeding of the 31st International Conference on Ocean, Offshore and Arctic Engineering*, pp. 369–380, 2012.
- [2] Y. L. Shao and O. M. Faltinsen, “A harmonic polynomial cell (HPC) method for 3D Laplace equation with application in marine hydrodynamics,” *Journal of Computational Physics*, vol. 274, pp. 312–332, 2014.
- [3] H. Liang, O. M. Faltinsen, and Y.-L. Shao, “Application of a 2D harmonic polynomial cell (HPC) method to singular flows and lifting problems,” *Applied Ocean Research*, vol. 53, pp. 75–90, 2015.
- [4] F. C. W. Hanssen, A. Bardazzi, C. Lugni, and M. Greco, “Free-surface tracking in 2D with the harmonic polynomial cell method: Two alternative strategies,” *International Journal for Numerical Methods in Engineering*, vol. 113, no. 2, pp. 311–351, 2018.
- [5] S. Ma, F. C. W. Hanssen, M. A. Siddiqui, M. Greco, and O. M. Faltinsen, “Local and global properties of the harmonic polynomial cell method: In-depth analysis in two dimensions,” *International Journal for Numerical Methods in Engineering*, vol. 113, no. 4, pp. 681–718, 2018.
- [6] A. Savitzky and M. J. E. Golay, “Smoothing and differentiation of data by simplified least squares procedures.,” *Analytical Chemistry*, vol. 36, no. 8, pp. 1627–1639, 1964.
- [7] A. P. Engsig-Karup, H. B. Bingham, and O. Lindberg, “An efficient flexible-order model for 3D nonlinear water waves,” *Journal of Computational Physics*, vol. 228, no. 6, pp. 2100–2118, 2009.
- [8] J. N. Newman, “Analysis of wave generators and absorbers in basins,” *Applied Ocean Research*, vol. 32, no. 1, pp. 71–82, 2010.